Journal of Materials Chemistry B

ROYAL SOCIETY OF CHEMISTRY

PAPER

View Article Online
View Journal

Cite this: DOI: 10.1039/d5tb02880a

Impact of 2′-fluoro nucleobase modifications on CD detection, sensitivity and specificity of short oligonucleotides bound to alginate hydrogels

Daisee K. Lubrin, [a] Colin I. Elliott, [a] Jean-Paul Desaulniers [b] and Theresa Stotesbury *[b]

Chemical modification of oligonucleotides has aided in the advancement of various therapeutic applications; however, their impact on biosensor performance remains understudied. As demand grows for rapid, sensitive, and portable detection technologies in healthcare, environmental, and forensic fields, leveraging the effects of chemical modifications with spectroscopic detection methods offers an opportunity to improve biosensor performance. Herein, we synthesize label-free oligonucleotide-bound alginate hydrogels as biosensors and use circular dichroism (CD) spectroscopy to detect and confirm DNA and RNA hybridization without amplification or labelling. We particularly focus on the impact of 2′-fluoro modifications on biosensor sensitivity and specificity. Fluorine-modified DNA-based biosensors demonstrate more than a threefold increase in sensitivity compared to unmodified DNA. RNA-based biosensors displayed a similar trend, where 2′-fluoro nucleobase modifications significantly lowered the LOD. Biosensor specificity is evaluated by adding mixtures containing up to four non-complementary strands to the alginate-oligo hydrogels. Fluorine-modified biosensors consistently demonstrated greater specificity with more distinct shifts in CD spectra compared to unmodified DNA. Principal component analysis was applied to differentiated samples with and without a bound complement. Additionally, when thermal melt data was combined with CD spectral data it was possible with a random forest model to predict whether unknown samples demonstrated complement binding, with accuracies of 95% and 83% for 2′-F modified and unmodified oligos, respectively. Our findings highlight the enhancement in biosensor sensitivity and specificity conferred by 2′-fluoro modifications, demonstrating their potential for improved label-free, amplification-free detection of oligonucleotides in complex environmental and forensic samples.

Received 22nd December 2025,
Accepted 24th March 2026

DOI: 10.1039/d5tb02880a

rsc.li/materials-b

1. Introduction

Biosensors traditionally consist of a target, a probe/bioreceptor, and a transducer, where the signal transducer converts the bio-recognition event (*i.e.*, binding of probe to the target) into a measurable signal.[1] Biosensor design can vary, where the probe could be cells, enzymes, aptamers, or nucleic acids, with responses most often transduced and recorded *via* optical, electrochemical, or acoustic means.[1–3] Low analyte concentrations and complex sample matrices are often encountered, leading to increased demand for sensitive, specific, and selective biosensors.[4] Oligonucleotides, particularly DNA, have attractive properties for hydrogel and biosensor synthesis, such as biocompatibility, specific base-pairing, programmability, tunability, and high thermal stability.[5] Hydrogels are three-dimensional cross-linked structures with high water content that can be synthesized using various synthetic and natural polymers.[6–9] DNA can serve as (i) the polymer backbone of the hydrogel, typically formed through self-assembly and hybridization of complementary strands, (ii) functionalized cross-linkers, or (iii) bioactive molecules rather than structural elements.[19] Oligonucleotide-based biosensors are used in various applications, including the sensitive and selective detection of genetic targets, including but not limited to *in vitro* diagnostics and environmental hazard detection,[10,11] clinical diagnostic tests for viral respiratory illnesses,[12,13] diseases,[7] and the detection of forensically relevant metabolites from seized evidence.[14] These biosensors traditionally depend on labelling, amplification, and/or immobilization for detection and signal transduction, which have drawbacks.[2] Labelling approaches, such as the use of molecular beacons,

[a] *Applied Bioscience Graduate Program, Faculty of Science, Ontario Tech University, 2000 Simcoe St N, Oshawa, Ontario, L1G 0C5, Canada. E-mail: theresa.stotesbury@ontariotechu.ca*
[b] *Faculty of Science Ontario Tech University, 2000 Simcoe St N, Oshawa, Ontario, L1G 0C5, Canada*

fluorescent tags, fluorophores, or quantum dots, can be challenging, expensive, and time-consuming, while increasing background fluorescence and steric hindrance, reducing the bioaffinity of the probe.[4,15,16] Stimuli-responsive DNA hydrogels are often self-assembled through various amplification techniques, but require complicated steps and produce gels with low mechanical strength.[17] Further, amplification of target oligos by polymerase chain reaction (PCR) or isothermal amplification requires multiple sets of specific primers and enzymes,[18] which could be prone to off-target effects, primer dimerization, or low amplification efficiency in the presence of inhibitors.[19] Electrochemical detection is often used to transduce bio-recognition events, but requires conductive materials, oligo immobilization, and functionalization of electrode and/or sensor surfaces, resulting in complex and costly synthesis.[15] The development of a label-free, amplification-free, and immobilization-free oligonucleotide-based biosensor could circumvent these challenges.

Oligonucleotides can be chemically modified for various applications, altering their structure and function,[20–24] but improving nucleotide stability, binding affinity, pharmacokinetic properties and/or nuclease resistance.[23,24] The phosphate backbone, sugar moiety, and nucleobase can all be altered based on the desired application (often therapeutic).[23,24] However, the impact of these chemical modifications on biosensor performance remains largely understudied, prompting us to investigate how these modifications can be harnessed to enhance detection capabilities without the need for labelling, amplification, or immobilization. Fluorine-modified oligonucleotides are of particular interest and contain a fluorine atom at the C2′ carbon of the sugar moiety. The high polarity of fluorine attracts the C2′ carbon[20] of the deoxyribose sugar of the oligonucleotide, causing it to adopt the standard and more stable C3′-endo pucker,[20] where the 3′ carbon bends into the ring, and the bases are oriented further from the helical axis.[25] The strong electronegativity of fluorine stabilizes the C3′-endo sugar pucker,[26] creating more polarized nucleobases. This strengthens Watson–Crick base pairing and enhances base stacking,[22,27] leading to increased chirality in the molecule. In addition, the 2′-fluoro nucleobase modifications increase nuclease resistance,[28,29] affinity to target molecules,[28] and the stability of the duplex,[30] which are important considerations in biosensor synthesis. The altered nucleic acid structure and hybridization dynamics could result in more pronounced changes in circular dichroism (CD) spectral signatures. CD is an absorption spectroscopy technique that measures the differential absorption of left and right-circularly polarized light to probe optically active chiral structures. The addition of 2′-fluoro modifications into the oligonucleotide probe of a biosensor could therefore provide a novel, cost-effective way of improving its sensitivity and specificity by capitalizing on these effects.

In this study, we synthesized and evaluated the performance of short oligonucleotide-bound alginate hydrogels as biosensors, with a particular focus on enhancing sensitivity and specificity through 2′-fluoro nucleobase modifications. Alginate is a negatively charged polysaccharide derived from brown algae and is composed of α-L-guluronic and β-D-mannuronic acid residues.[31] Alginate-based hydrogels exhibit low toxicity, high biocompatibility, and are easily physically and chemically modified.[31] The mechanical, viscoelastic, self-healing, and degradation properties of alginate can be tailored to exhibit various functions.[32–34] Ionic crosslinking of alginate with divalent cations is the most common method of gelation due to its simplicity and mild reaction conditions;[35] however, these ionically crosslinked gels lose their mechanical strength over time.[36] To overcome this loss of mechanical strength, covalently crosslinked hydrogels can be synthesized with crosslinkers[33] such as DNA and RNA. These could further be used as bioinert, biocompatible, biodegradable, and low-cost biosensors with a microstructure resembling the extracellular matrix.[31,37] Our biosensor was label-free, amplification-free, and synthesized without a traditional internal signal transducer. Rather, we leveraged the intrinsic chirality and arrangement of nucleobases in oligonucleotides, measuring hybridization to the target oligo with CD spectroscopy[38] and exploited the effects of 2′-fluoro nucleobase modifications to enhance biosensor sensitivity and specificity.[38]

2. Experimental section

2.1. Materials

2.1.1. EDC/NHS coupling reaction. Alginic acid sodium salt for brown algae (Sigma; Ontario, Canada), monohydrate free acid (MES) (MP Biomedicals Inc.; California, USA), 2-azidoethanamine, sodium hydroxide (Sigma; Ontario, Canada), 1-(3-dimethylaminopropyl)-3-ethylcarbodiimide hydrochloride (EDC) (Tokyo Chemical Industry; Ontario, Canada), *N*-hydroxysuccinimide (NHS) (Sigma; Ontario, Canada), Amicon Ultra-0.5 Centrifugal Filter Unit (3 kDa MWCO) (Sigma; Ontario, Canada), 11-azido-3,6,9-trioxaundecan-1-amine (Sigma; Ontario, Canada), Amicon Ultra-4 centrifugal filter unit (Sigma; Ontario, Canada), *N*-hydroxysulfosuccinimide sodium salt (Sulfo-NHS), 97% (Thermo Scientific; Ontario, Canada).

2.1.2. CuAAC reaction. Copper(II) sulfate (Sigma; Ontario, Canada), sodium-L-ascorbate (Sigma; Ontario, Canada), tris(3-hydroxypropyltriazolylmethyl)amine (Sigma; Ontario, Canada), aminoguanidine hydrochloride (Sigma; Ontario, Canada), potassium phosphate monobasic (Thermo Scientific; Ontario, Canada), sodium hydroxide (Sigma; Ontario, Canada).

2.2. Synthesis of the alginate-azide hydrogel

We performed an EDC/NHS coupling reaction adapted from Shi *et al.*[39] Briefly, sodium alginate solution (1% w/v) was prepared by dissolving 50 mg (6.68×10^{-2} mM) alginic acid sodium salt from brown algae in 5 mL of 50 mM (2.50×10^{-1} mM) MES Buffer of pH 5.[39] The solution was stirred overnight to ensure that it had completely dissolved. 0.116 g of EDC (0.74 mM) and 0.026 g sulfo-NHS (0.12 mM) were added to the alginate dissolved in MES buffer 5 mL and reacted for 30 min. 28 μL volume of crosslinker, 2-azidoethanamine (0.33 mM), and 55 μL of 6 M (1.32 mM) NaOH of pH 8 were subsequently added and left to react at room temperature for 24 hours.[39] A crosslinker-free control was also synthesized with the same

concentrations of reagents, but without the 2′-azidoethanamine crosslinker. The Amicon 4K Centrifugal Filter Unit filtered the solution at 12 000 rpm for 15 mins at 22°C. Each hydrogel was washed twice with Milli Q water and collected from the filter.

2.2.1. Characterization of alginate-azide hydrogel

2.2.1.1. Fourier-transform infrared spectroscopy (FTIR). A Bruker ALPHA-P compact FTIR spectrometer was used to collect spectra for each of the dried hydrogels. Three drops of each cleaned product were placed in a Petri dish (3 replicates) and air-dried overnight. Each replicate was scanned on the FTIR spectrometer using the ATR crystal over 400 to 4000 cm^{-1}. Both background scans and sample scans were measured at a resolution of 4 cm^{-1} at 0.75 Hz for a total of 5 scans collected per sample.

2.2.1.2. Nuclear magnetic resonance (NMR) spectroscopy. We acquired ^{1}H NMR and ^{13}C NMR spectra of the hydrogels using a 400 MHz Bruker IconNMR™ spectrometer. The hydrogels were prepared by drying the cleaned product from 2.2 at 50 °C using a Genevac™ miVac centrifugal concentrator. Dried hydrogels (25–40 mg) were dissolved in approximately 0.5 mL of D_2O and placed in an NMR glass tube for analysis. 40 and 12 500 scans were collected per sample for ^{1}H NMR and ^{13}C NMR, respectively, at a frequency of 100.67 MHz. ^{13}C NMR spectra were recorded with a sweep width of 24037.73 Hz.

2.2.1.3. Rheological characterization. We diluted (1 : 4) alginate-azide hydrogel with Milli-Q® water to reduce the viscosity of our product and avoid wall slip during rheological measurements. A TA Instruments DHR20 stress-controlled rheometer with an advanced Peltier plate and solvent trap system was used to perform an amplitude sweep from 0.01% to 100% at a fixed angular frequency of 6.28 rad s^{-1}, while frequency sweeps were performed at 22 °C from 0.01 rad s^{-1} to 150 rad s^{-1} at a constant strain amplitude of 0.5%. Flow sweeps were acquired from 1–1200 s^{-1} to measure viscosity.

2.3. DNA/RNA synthesis

Oligonucleotide strands were either (1) created in our lab using a 394 Applied Biosystems DNA/RNA synthesizer or K&A Synthesizer using standard DNA and RNA phosphoramidites and an alkynyl phosphoramidite from ChemGenes or (2) purchased from Integrated DNA Technologies (IDT) (Ontario, Canada) (Table 1). Three strands with non-complementary sequences (to the DNA Probe strand) were synthesized or purchased. The Scrambled A strand contained the same nucleotides as the DNA Target strand, but with a randomly scrambled sequence. Scrambled B and Scrambled C have a 5′ alkyne functionality, and different nucleotide compositions than the DNA Target strand. The mismatched strand is identical to the DNA Target, except for three mismatched nucleotides in the middle of the sequence (Table 1). Two thymine nucleotides were incorporated at the 3′ end of the RNA strands.

2.4. Copper-catalyzed azide–alkyne cycloaddition (CuAAC) reaction

We adapted the copper-catalyzed azide–alkyne cycloaddition (CuAAC) described in Presolski *et al.*[40] 0.0042 g of alginate-2-azidoethanamine (alginate-azide) hydrogel was dissolved in 114 μL (11.4 nM) of phosphate buffer. 20 nmol of DNA/RNA/2′-F Oligo-Probe strand and 2.5 μL of Solution 1–7.5 μL (0.75 nM) of $CuSO_4$ and 1.5 μL (0.75 nM) of THPTA – were added to the dissolved alginate-azide. 8.33 μL (41.65 nM) of aminoguanidine HCl and 8.33 μL (41.65 nM) of sodium ascorbate were subsequently added. Reagents were allowed to react for 1 hour on a stir plate at 40 °C, then transferred into a 50 kDA MWCO Amicon ultra 0.5 mL centrifugal filter and centrifuged at 12 000 rpm at 40 °C for 15 min. The filter column was washed twice with 300 μL of sterile water and spun again at the same conditions for 15 min. The filtrate and liquid remaining in the filter were transferred to separate 1.5 mL microcentrifuge tubes. 400 μL of water was added to the small volume (<10 μL) of product remaining in the filter and mixed by pipetting prior to collection.

Table 1 Sequences of the oligonucleotide strands used in biosensor synthesis. In the mismatch strands, the mismatched nucleotides are bolded and underlined. Thymine nucleotides at the 3′ end of RNA strands are designated as "t". 2′-fluorine-modified bases have an "F" subscript

Strand	Sequence
DNA probe	5′-(Alkyne)-ATTTCCTGTGTCAGACCCTGtt-3′
DNA target	5′-CAGGGTCTGACACAGGAAATtt-3′
RNA probe	5′-(Alkyne)-CUUACGCUGAGUACUUCGAtt-3′
RNA target	5′-UCGAAGUACUCAGCGUAAGtt-3′
Scrambled A	5′-GGCCTTCACTCGTATGTTATTC-3′
Scrambled B	5′-(Alkyne)-ATTGCGGACTCGATACGATCAT-3′
Scrambled C	5′-(Alkyne)-CAGTCGGTAGTGATATGGCATT-3′
Mismatch (3)	5′-CAGGGTC**G**N**A**CA**G**AGGAAATtt-3′
Mismatch (5)	5′-CAGGGTC**G**N**A**CA**G**A**N**N**A**AATtt-3′
Mismatch (7)	5′-CAGG**A**A**C**G**T**N**A**CA**G**A**N**N**A**AATtt-3′
Mismatch (9)	5′-CAGG**A**A**C**G**T**N**A**CA**G**A**N**N**A**H**H**Ttt-3′
2′-F oligo (F-3)	5′-(Alkyne)-ATT$_F$TCCTGTGT$_F$CAGACCCT$_F$Gtt-3′
2′-F oligo (F-6)	5′-(Alkyne)-ATTTCCTGT$_F$G$_F$T$_F$C$_F$A$_F$G$_F$ACCCTGtt-3′
2′-F oligo (F-14)	5′-(Alkyne)-A$_F$T$_F$T$_F$T$_F$C$_F$CTGT$_F$G$_F$T$_F$C$_F$A$_F$G$_F$ACCC$_F$T$_F$G$_F$tt-3′
2′-F oligo (F-All$_{DNA}$)[a]	5′-(Alkyne)-A$_F$T$_F$T$_F$T$_F$T$_F$C$_F$C$_F$T$_F$G$_F$T$_F$G$_F$T$_F$C$_F$A$_F$G$_F$A$_F$C$_F$C$_F$C$_F$T$_F$G$_F$tt-3′
2′-F oligo (F-All$_{RNA}$)[a]	5′-(Alkyne)-C$_F$U$_F$U$_F$A$_F$C$_F$G$_F$C$_F$U$_F$G$_F$A$_F$G$_F$U$_F$A$_F$C$_F$U$_F$U$_F$C$_F$G$_F$A$_F$tt-3′

[a] All bases in 2′F oligo (F-All$_{DNA}$) and 2′F oligo (F-All$_{RNA}$) are 2′F modified except the two thymine bases at the 3′ end.

2.4.1. Circular dichroism (CD) spectroscopy. 400 μL of the product from Section 2.4 was transferred to a 400 μL rectangular quartz cuvette with a 1 mm path length. CD spectra were acquired in triplicate using a Jasco J-815 CD spectropolarimeter at 20 °C, recorded every 0.2 nm from 200 to 300 nm at a scanning rate of 100 nm min^{-1}. The change in absorbance was measured against a change in CD (mdeg). Samples were automatically baseline-corrected by analyzing the solvent (CD buffer) before each sample measurement. A moving average with a window size of 25 was used to smooth each spectrum.

2.5. Sensitivity and specificity studies

2.5.1. 2′-F modification. The CuAAC reaction described in Section 2.4 was performed with oligonucleotide sequences containing varying amounts of 2′-fluorine-modified bases (Table 1). For each of these reactions, 20 nmol of the fluorine-modified oligo was covalently bound to the alginate-azide hydrogel. The following 2′-F Oligo sequences were tested: 2′-F Oligo (F-3), 2′-F Oligo (F-6), 2′-F Oligo (F-16), 2′-F Oligo (F-All_{DNA}). CD spectra were acquired to confirm the binding of ss2′-F Oligo to the alginate-azide. An equimolar amount (20 nmol) of the DNA Target was added to the probe-containing alginate-azide hydrogel. The hydrogel was placed in a 94 °C water bath for 2 minutes before cooling at room temperature overnight to ensure annealing. CD spectra were collected for each sample as described in Section 2.4.1. As a control, identical hybridization experiments were performed using the same 2′-F-modified sequences free in solution without the CuAAC conjugation to alginate. In these experiments, 20 nmol of probe and equimolar target were annealed under the same thermal conditions, and CD spectra were acquired as described in Section 2.4.1.

2.5.2. Sensitivity studies. Two different sensitivity studies were performed. In the first, the CuAAC reaction described in Section 2.4 was repeated with varying amounts of DNA (0–83.3) nmol, RNA (0–40) nmol, 2′-F Oligo (F-All_{DNA}) (0–20) nmol, and 2′-F Oligo (F-All_{RNA}) (0–20) nmol. CD spectra were first acquired to confirm the binding of single-stranded (ss) DNA/RNA (*i.e.*, Probe strand) to the alginate-azide. An equimolar amount of DNA/RNA complement strand (either 1.25, 2.5, 5, 10, 20, 30, 40, 60 or 83.3) nmol was added to the Probe strand-containing alginate-azide hydrogel. In the second study, the amount of Probe remained constant while the amount of target varied. The CuAAC reaction described in Section 2.4 was repeated with constant amounts of DNA, RNA, 2′-F Oligo (F-All_{DNA}), and 2′-F Oligo (F-All_{RNA}) (10 nmol). An increasing amount of DNA/RNA Target strand (1.25, 2.5, 5, 10, or 20) nmol was added to the probe-containing alginate-azide hydrogel. In both studies, the hydrogel containing the added complementary strand was placed in a 94 °C water bath for 2 minutes prior to cooling at room temperature overnight to ensure annealing. CD spectra were recorded to confirm complementary binding. Limits of detection (LOD) for the different types of oligo hydrogels were calculated using 3.3 standard deviations of the intercept and the slope of the regression line.[41] For comparison to previous literature, the molar LOD amounts were converted to molarity using a volume of 400 μL (volume requirement for CD spectroscopy measurements). The total amount of oligonucleotide added during the click chemistry reaction was used rather than the amount that was successfully conjugated, providing a conservative estimate of sensitivity that accounts for variability in conjugation efficiency.

2.5.3. Specificity study. Combinations of equimolar amounts (*i.e.*, 20 nmol each) of DNA Target, scrambled, and mismatched strands were added to the alginate-ssDNA hydrogel to determine its specificity for its complement (Table 2). CD spectra were collected to assess the binding specificity in each hydrogel. This was repeated with 10 nmol of 2′-F Oligo (F-All_{DNA}) rather than the DNA probe.

2.5.4. Mismatch determination threshold study. Combinations of equimolar amounts (*i.e.*, 10 nmol each) of DNA Target, and various mismatched strands were added to the alginate-ssDNA hydrogel to determine the mismatch threshold for discrimination between the perfectly complementary target

Table 2 Types of complement strands added to each hydrogel of the specificity study. Each hydrogel contained the Probe strand (either unmodified DNA or 2′-F Oligo (F-All_{DNA}))

Sample #	DNA contained in each hydrogel
1	No DNA
2	DNA target strand
3	Mismatch
4	Mismatch + DNA target strand
5	Scrambled A
6	Scrambled A + DNA target strand
7	Scrambled B
8	Scrambled B + DNA target strand
9	Scrambled C
10	Scrambled C + DNA target strand
11	Scrambled B + scrambled C
12	Scrambled B + scrambled C + DNA target strand
13	Scrambled A + scrambled B + scrambled C
14	Scrambled A + scrambled B + scrambled C + DNA target strand
15	Mismatch + scrambled A
16	Mismatch + scrambled A + DNA target strand
17	Mismatch + scrambled A + scrambled B + scrambled C
18	Mismatch + scrambled A + scrambled B + scrambled C + DNA target

Table 3 Types of complement strands added to each hydrogel of the mismatch determination threshold study

Sample #	DNA contained in each hydrogel
1	No DNA sense
2	DNA target strand
3	3 mismatch sequence
4	3 mismatch sequence + DNA target strand
5	5 mismatch sequence
6	5 mismatch sequence + DNA target strand
7	7 mismatch sequence
8	7 mismatch sequence + DNA target strand
9	9 mismatch sequence
10	9 mismatch sequence + DNA target strand

and sequences containing mismatches (Table 3). CD spectra were collected to assess the binding specificity in each hydrogel.

2.5.5. Thermal denaturation studies. Thermal denaturation studies were performed on samples from the specificity study using a Jasco J-815 CD Spectropolarimeter equipped with a temperature controller. Melting temperature (T_m) was determined by measuring UV absorbance at 260 nm while the temperature was increased from 10 to 95 °C at a rate of 0.5 °C per minute. Technical replicates were conducted by reannealing the strands by placing the sample in a 94 °C water bath for 2 minutes and then cooling to room temperature overnight. T_m data was analyzed using Meltwin v3.5 software.

2.5.6. Statistical analyses. Origin Lab software (2024b) was used to plot all spectral data. Peak identification and maximum absorption wavelength (λ_{max}) were recorded from the ATR-FTIR and CD spectra. Statistical analyses were completed using R-Studio Software (Version 4.2.2). Principal component analysis (PCA) was performed on CD spectra obtained from sensitivity and specificity studies to determine whether hydrogels clustered according to various physicochemical properties (*e.g.*, type of oligo, conformation, complement binding, *etc*). Each spectrum was normalized to its maximum ellipticity value based on sample type prior to PCA and random forest (RF) computation. RF models were built with 1000 decision trees and trained with different values of mtry (number of variables to randomly sample as candidates at each split) and optimized using *k*-fold ($k = 5$) cross-validation. The optimized model was then used for predictions. Data was randomly split into a training and testing set: 4/5 of the data was allocated to the training set, while the remaining 1/5 made up the testing set. Prediction accuracy was computed by comparing model classification of test data (*i.e.*, withheld data) with their true classification (*i.e.*, with or without complement).

3. Results and discussion

3.1. Binding of functionalized oligos to alginate-azide

Alginate-oligonucleotide hydrogels were recovered from the filter as residue. The molecular weight of the hydrogel, which comprises the oligonucleotide bound to the alginate-azide backbone, is too large to pass through the centrifugal filter membrane. This format enables effective immobilization of the target sequence and facilitates separation of bound target from unbound or noncomplementary strands. In addition, the hydrogel matrix protects against enzymatic degradation[42] which may be advantageous for future applications involving sample types where nuclease exposure is expected.

DNA and RNA binding to the alginate-azide hydrogel was confirmed by characteristic changes in CD spectra (Fig. 1). Alginate-azide displayed a single peak at ~200 nm and no significant ellipticity bands between 210 nm and 300 nm due to the lack of secondary structure. DNA was successfully bound to the alginate-azide, as observed by the positive bands at 220 nm and 260 nm to 280 nm, and a negative band at 245 nm, typical of B-form DNA (Fig. 1b, and d).[43] These bands displayed larger ellipticity values, blue-shifted maxima, and long-wavelength crossovers upon DNA duplex formation (Fig. 1d), indicative of successful hybridization between the target and the probe strand.[43–45] RNA was also successfully bound to the alginate-azide as observed by the positive band at 260 nm and a negative band at 210 nm (Fig. 1c), consistent with the A-form helix of dsRNA.[45,46] Both bands had greater ellipticity magnitudes for alginate-dsRNA than alginate-ssRNA, indicating a shift from ssRNA to dsRNA upon hybridization (Fig. 1e). Like DNA, RNA could also be detected in the filtrate (Fig. S4; filtrate), suggesting that only alginate-azide-bound RNA remained in the filter residue.

3.2. Impact of 2′-fluorine modifications on CD response

The distortion of Watson–Crick base pairs[47] and nucleobase stacking[27] are known to influence CD spectra and are affected by the addition of the highly electronegative fluorine atom. An increase in the number of fluorinated bases in the Probe strand bound to alginate resulted in an increased CD signal intensity and a progressive blue shift in the peak maxima. The unmodified DNA probe displayed the lowest intensity and the most red-shifted peak, while 2′-F Oligo (F-All$_{DNA}$) displayed the greatest intensity and most blue-shifted peak. As the degree of 2′-F substitution increased, the peak maximum shifted from 279.7 nm to 268.2 nm (Fig. 2a). CD response was further enhanced and continued to blue-shift upon hybridization with the complementary unmodified DNA target (Fig. 2b), with the peak shifting to 264.4 nm. Notably, the CD signal intensity for the 2′-F Oligo (F-All$_{DNA}$) + DNA target complex was approximately three times higher than that of the unmodified DNA probe + DNA target complex. Similar results were also observed in the CD signatures of these free probe sequences (not bound to the alginate-azide) (Fig. S5). This suggests that oligo modification with fluorine could significantly enhance the sensitivity of our biosensor.

3.3. Sensitivity studies

3.3.1. Sensitivity study I – equimolar amounts of probe and target. The average LOD of the alginate-DNA biosensor was 8.1 nmol (20 μM), while the LOD for the 2′-F Oligo (F-All$_{DNA}$) was 2.3 nmol (5.6 μM), meaning that 2.3 nmol of duplex is required to obtain an observable signal. Peaks expected of ssDNA and dsDNA begin to appear at a concentration of 5 nmol and are clearly visible by 10 nmol, while peaks for ss2′-F Oligo

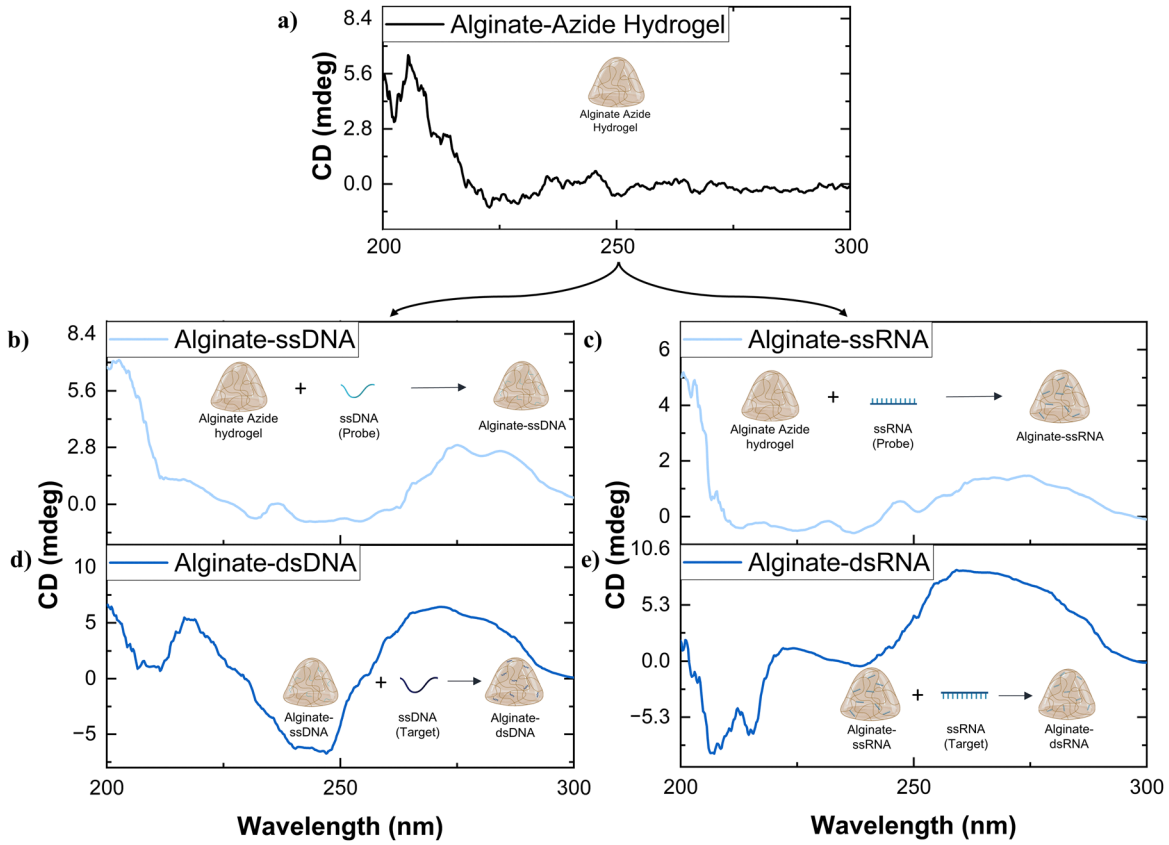

Fig. 1 Example CD spectra from (a) alginate-azide, (b) alginate-ssDNA, (c) alginate-ssRNA, (d) alginate-dsDNA, and (e) alginate-dsRNA hydrogels collected from the centrifugal filter (*i.e.*, residue). Single-stranded hydrogels contain the Probe strand, while double-stranded (ds) hydrogels include the duplex produced by hybridization of the complementary Target strand.

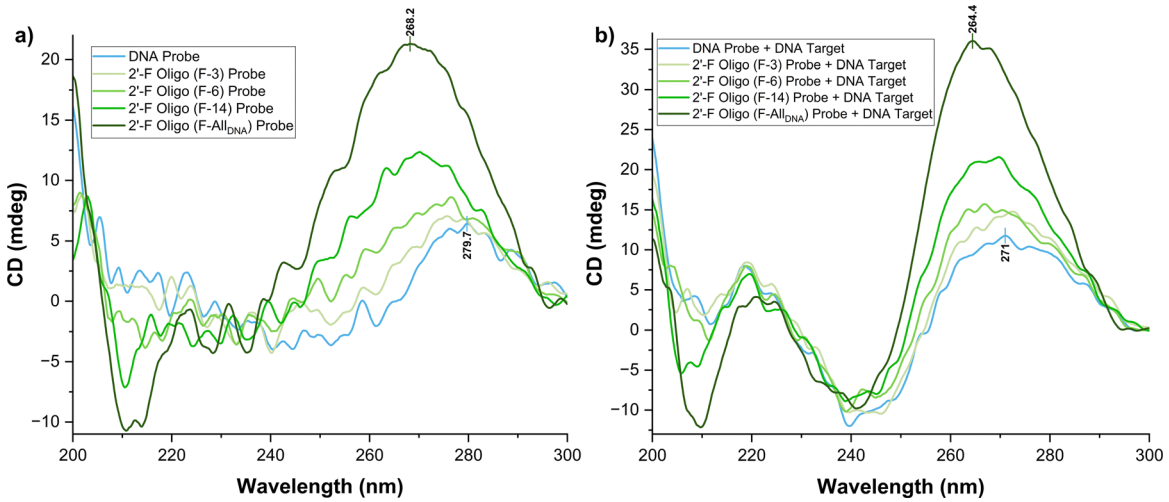

Fig. 2 CD spectra of (a) probe sequences with an increasing number of 2′-fluoro modified bases bound to alginate and (b) the corresponding duplexes with the DNA target strand as the complement.

(F-All$_{DNA}$) and ds2′-F Oligo (F-All$_{DNA}$) appear at 2.5 nmol and were clearly visible by 5 nmol, corroborating our computed LOD values (Fig. S6 and S8 respectively). Similar results were obtained for alginate-RNA hydrogels (Fig. S7 and S9), with a LOD of 4.6 nmol (12 μM) for unmodified RNA and 1.7 nmol (4.6 μM) for 2′-F Oligo (F-All$_{RNA}$). 2′F nucleobase modifications led to a greater increase in the sensitivity of DNA than RNA biosensors. The strong electronegativity of the fluorine atom on the 2′ position of the sugar significantly influences sugar puckering, favouring a C3'endo conformation.[29] This impacts

the stability and structure of the duplex,[48] altering base stacking by disrupting the N-glycosidic bond orientation stacking,[27] resulting in deviations from the classical helical structure. These structural changes are reflected in variations in CD signatures. DNA typically adopts a C2′-endo sugar pucker while RNA naturally assumes a C3′-endo conformation.[25] The electronegativity of the 2′-fluoro group also more closely resembles that of the 2′-hydroxyl group in RNA than the 2′-hydrogen in DNA. This can be expected to enhance nucleobase polarization, increase Watson–Crick H-bonding strength, and increase enthalpic stabilization due to improved stacking in 2′-F Oligo (F-All$_{DNA}$) relative to 2′-F Oligo (F-All$_{RNA}$).[29] Therefore, fluorine modifications induce more substantial conformational and stacking disruptions in DNA compared to RNA, influencing chirality and, ultimately, biosensor sensitivity. Lower LODs have previously been reported for DNA- and RNA-based biosensors, but those relied on more complex and challenging synthesis and detection techniques, such as immobilization, tagging and/or amplification,[2,15,49] compared to the simpler label-free, amplification-free approach used in our study (Table 4).

PCA revealed that samples containing unmodified *versus* 2′F-modified oligos could be distinguished, highlighting the influence of fluorine modification on CD spectra (Fig. 3c). This can be explained due to the natural C2′endo conformation of DNA, which must now reorganize its conformation to C3′-endo when paired with the 2′-F-modified oligo to maximize complementary binding thermodynamics. On the other hand, RNA samples did not cluster as distinctively, and demonstrated some overlap in points and ellipses, likely due to their pre-organized C3′-endo conformation (Fig. 3d). Nevertheless, for both DNA and RNA samples, single-stranded 2′F-oligo probes exhibited greater similarity to their double-stranded counterparts and clustered closer together than the unmodified oligonucleotides, likely resulting from the blue shifts in the CD maxima caused by 2′-fluoro nucleobase modifications. Unmodified ssDNA exhibits a CD maximum at 280 nm compared to its dsDNA counterpart at 272.6 nm (Fig. S6). The introduction of 2′-fluoro modifications induces significant structural changes, leading to a CD maximum of 265 nm for both ss 2′-F Oligo (F-All$_{DNA}$) samples and ds 2′-F Oligo (F-All$_{DNA}$) samples (Fig. S6). The wavelengths contributing to the highest variance among samples and used to separate them in the PCA were 259–262 nm and 275–290 nm for dimension 1, and 237–245 nm for dimensions 2. These represent the regions where the wavebands cross the *x*-axis on either side of the positive peak. In unmodified RNA, the ss and ds conformations have peaks at 272 and 262 nm, respectively, while the fluorine modifications shift the CD maxima to 264 and 265 nm, respectively (Fig. S7). The wavelengths contributing to the separation of the samples in the PCA were 216–231 nm (*i.e.*, region of the spectra where the negative peak approaches the *x*-axis) for dimension 1 and 253–263 nm (*i.e.*, region of the spectra where the left side of the positive peak approaches the *x*-axis) for dimension 2. Although data were normalized to the maximum peak intensity, slight tailing persists in these regions and contributes to the variance detected by the PCA.

Table 4 Comparison of the performance of the proposed biosensor with other reported biosensors for oligonucleotide detection

Type of biosensor	Probe/target	LOD	Benefit	Drawbacks
Electro-chemical[50]	Probe: DNA on PEG/Ppy nanowire Target: miRNA	0.33 pM	• Long linear range	• Relatively complicated design • Requires skilled personnel for operation
Electro-chemical – differential pulse voltammetry (DVP)[51]	Probe: DNA on MXene w/Pt/C nanocomposite Target: RNA	0.4 aM	• 100% accuracy and 97.87% specificity • Long linear range	• Relatively complicated design
Electro-chemical – cyclic voltammetry[52]	Probe: DNA hairpin with methylene blue and ferrocene Target: DNA	10 pM	• No bulky equipment needed • Not affected by sample's light transmittance	• Requires labelling • Relatively complicated design • Response inversely proportional to [target] • 20% loss of signal with washing
Spectral (fluorescent)[53]	Probe: Fluorescein tagged single stranded DNA Target: DNA	15 pM	• High selectivity (single-mismatch discrimination) • Good linear range	• Requires PCR amplification • Requires skilled personnel for operation
Spectral (fluorescent)[54]	Probe: fluorophore labelled ssDNA Target: DNA	20 pM	• Multiplex detection of DNA • Good dynamic range	• Requires amplification • Requires skilled personnel for operation
Chiroptical (our work)	Probe: ssOligo Target: ssOligo	DNA: 9.5 μM 2′-F Oligo (F All$_{DNA}$): 7.3 μM RNA: 3.2 μM 2′F Oligo (F All$_{RNA}$): 5.3 μM	• Label-free • Amplification-Free • Relatively simple synthesis • Relatively low production cost • Simple operation • Reuseable	• Relatively high LOD

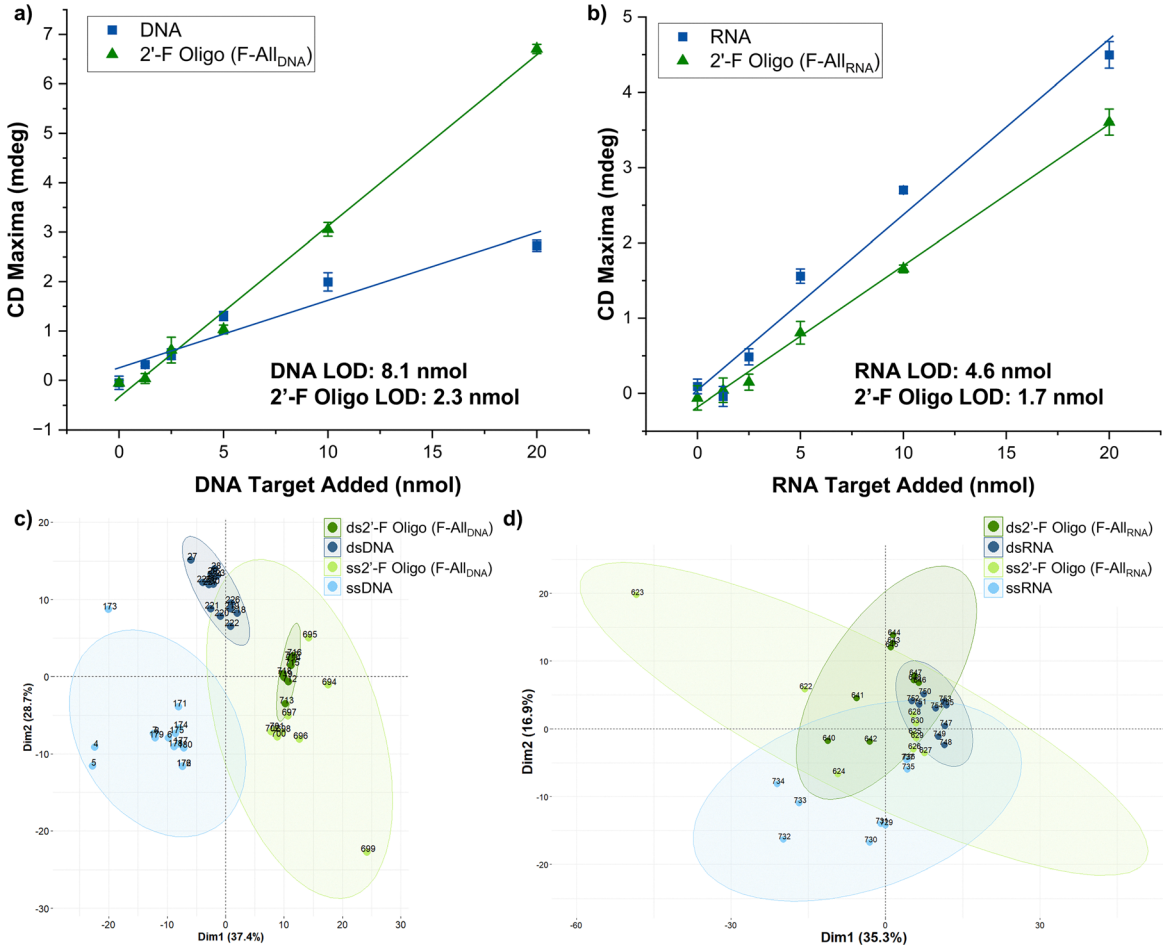

Fig. 3 Calibration curves of (a) DNA (slope: 0.136; R^2: 0.921) and 2′-F Oligo (F-All$_{DNA}$) (slope: 0.346; R^2: 0.993) and (b) RNA (slope: 0.233; R^2: 0.972) and 2′-F Oligo (F-All$_{RNA}$) (slope: 0.188; R^2: 0.996). PCA of ss and ds (c) DNA and 2′-F Oligo (F-All$_{DNA}$) and (d) RNA and 2′-F Oligo (F-All$_{RNA}$) for the sensitivity studies with equimolar amounts of probe and target oligonucleotides added. Ellipses represent the 95% confidence intervals around the mean (centroid) of each group. PCAs include samples containing 5–20 nmol of oligo. PCA samples and their descriptions are included in Table S1.

3.3.2. Sensitivity study II – constant probe and varying target sequence. We kept the amount of probe constant at 10 nmol (above the previously determined LOD), while varying the amount of probe from 0 to 20 nmol. Keeping the amount of probe constant while varying the target sequence better simulates real-world scenarios, where the probe and target are likely not present in equimolar amounts. By using data from the positive CD maxima, the LOD was determined to be 3.8 nmol (9.5 μM) for DNA and 2.9 nmol (7.3 μM) for 2′-F Oligo (F-All$_{DNA}$; Fig. 4a), indicating that 2.9 nmol of target is required for an observable signal when using 10 nmol of probe. 2′-F Oligo (F-All$_{DNA}$) exhibited a greater response at the 0 nmol target sequence concentration, representing a scenario where only the single-stranded probe was present (Fig. 4a). This elevated response persisted as the target sequence was added, resulting in an overall improved LOD for 2′-F Oligo (F-All$_{DNA}$). Additionally, the steeper slope observed for the 2′-F Oligo (F-All$_{DNA}$) calibration curve could be attributed to altered base stacking interactions between the probe and target sequence, which influence the chirality of the molecule and increase the CD response. These findings support the use of 2′-F modifications for enhancing the sensitivity of DNA biosensors. For RNA (Fig. 4b), the LOD was 1.3 nmol (3.2 μM) for unmodified RNA and 2.1 nmol (5.3 μM) for 2′-F Oligo (F-All$_{RNA}$). Similar calibration slopes were observed for RNA and 2′-F Oligo (F-All$_{RNA}$), suggesting that the introduction of the 2′-F modifications does not have a substantial effect on the CD response compared to unmodified RNA, likely due to RNA's preorganized C3′-endo conformation.

PCA revealed effective clustering, with clear separation between single-stranded and double-stranded unmodified samples (Fig. 4c and d). 2′-F modified Oligo clustered tightly and could be distinguished from unmodified DNA samples, indicating greater consistency among samples. Compared to modified RNA, 2′-F modified Oligo exhibited tighter clustering, which could be attributed to its longer linear range and differences in CD maxima, further supporting its use as a biosensor compared to RNA. Unmodified DNA samples with low amounts of the target sequence (specifically the 1.25 nmol sample, 777–779 in the PCA) demonstrated evidence of duplex formation, but were plotted away from the other dsDNA

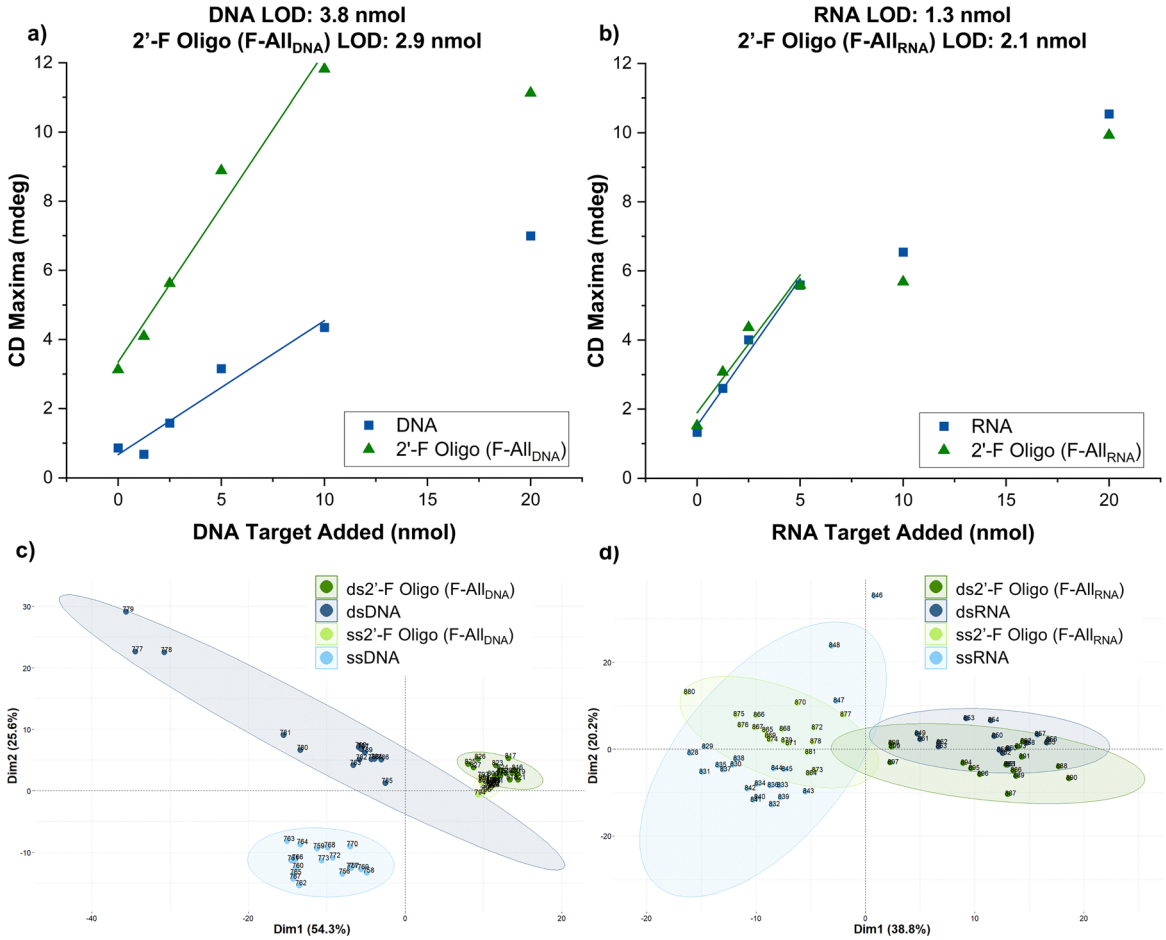

Fig. 4 Calibration curves of (a) DNA (slope: 0.388; R^2: 0.939) and 2′-F Oligo (F-All$_{DNA}$) (slope: 0.896; R^2: 0.970) at positive CD maxima, (b) RNA (slope: 0.851; R^2: 0.980) and 2′-F Oligo (F-All$_{RNA}$) (slope: 0.797; R^2: 0.947) at positive CD maxima. PCA of (c) ss and ds DNA and 2′-F Oligo (F-All$_{DNA}$) and (d) RNA and 2′-F Oligo (F-All$_{RNA}$) for Sensitivity Studies with constant probe and varying target sequence concentrations. PCAs include all samples containing 1.25–20 nmol of target sequence; CD response from 230–290 nm was used for PCA.

samples (Fig. 4c). However, for the 2′-F Oligo (F-All$_{DNA}$), all samples exhibited a duplex response greater than that of the single-stranded probe, leading to stronger contributions in the PCA. Single-stranded and double-stranded RNA samples clustered together, irrespective of fluorine modification, suggesting minimal effect of the 2′-F modifications on CD response, further corroborating the calibration curve in Fig. 4b. Unmodified and 2′-F Oligos were plotted together for comparative purposes. However, when plotted in separate PCAs, both unmodified and 2′-F modified Oligos had near complete separation based on conformation (*i.e.*, ss *vs.* ds) (Fig. S11 and S12). Despite the ss and ds CD maxima of 2′-F Oligos being closer together than their unmodified counterparts, this did not negatively affect target discrimination, and sample types were accurately identified at all target sequence concentrations.

3.4. Specificity study

Scrambled sequences were introduced in the form of mixtures to evaluate the binding specificity of DNA and 2′-F Oligo probes to the target DNA sequence. In both systems, the addition of scrambled sequences in the absence of the target sequence (Fig. 5a and d) produced spectra resembling that of the probe alone in both peak height and location, indicating a lack of binding affinity between the probe and non-complementary sequences. The long wavelength crossover underwent a red shift, contrary to the expected blue shift typically observed during the transition from single- to double-stranded DNA,[43] with this effect more pronounced in the 2′-F Oligo (F-All$_{DNA}$) compared to the unmodified DNA. To determine the mismatch discrimination threshold of the DNA probes, additional studies were conducted using target sequences containing 5, 7, and 9 mismatches (Fig. S13). These results demonstrated that when 5 or more mismatches were present in the target sequence, the corresponding CD spectra could be visually distinguished from samples containing a perfectly complementary target. We then analyzed a sequence with 3 mismatches to evaluate whether the 2′-F oligos displayed enhanced specificity in target binding. Partial binding was observed when a sequence with 3 mismatches was introduced Fig. 5a and b, top). The resulting spectra were more similar to Fig. 5b, top), the peak height for spectra with mismatched sequences (olive green) was between

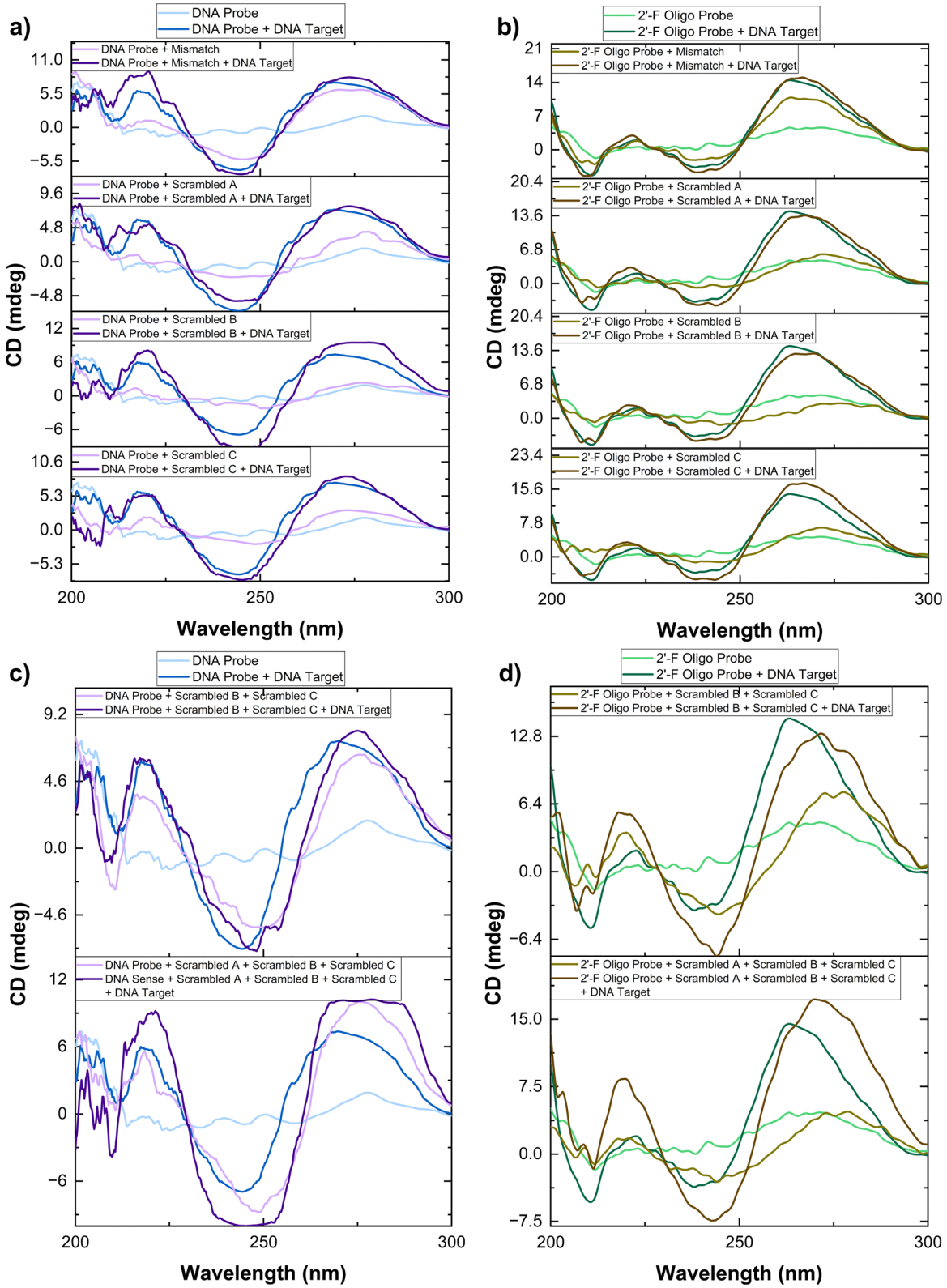

Fig. 5 CD spectra of the DNA hydrogels and 2′-F Oligo hydrogels tested during the specificity study. 2′-F Oligo corresponds to the 2′-F Oligo (F-ALL$_{DNA}$) sequence. Spectra are compared to Probe strands and a probe/target duplex, represented in light blue and dark blue for DNA and light green and dark green for 2′-F Oligo, respectively. CD Spectra in (a) and (b) represent samples with a single non-complementary sequence (*i.e.*, mismatch or scrambled), while spectra in (c) and (d) represent samples with multiple non-complementary sequences.

the single-stranded and double-stranded forms. This suggests that hydrogels incorporating 2′-F Oligos potentially offer greater discrimination between mismatched and perfectly complementary target sequences when only 3 bases are non-complementary, compared to those containing unmodified DNA probes. Although discrimination at 3 mismatches is not fully resolved by CD analysis alone, further evaluation using temperature melt analysis (Section 3.4.1) provides additional resolution between perfectly complementary and partially mismatched targets. Together, these results demonstrate robust visual discrimination at $\geq$5 mismatches, while enhanced discrimination at 3 mismatches is achieved when CD and thermal melt analyses are considered in combination.

Subtle differences were observed in CD spectra for larger mixtures containing two or three scrambled sequences with and without the target sequence (Fig. 5c and d). The peak heights of mixtures for unmodified DNA generally resembled those of hydrogels containing the probe-target duplex (Fig. 5c, light blue). The increased ellipticity near 270 nm in hydrogels containing both the probe and multiple scrambled sequences suggests partial duplex formation. Scrambled sequences B and C, containing eight complementary base pairs, might contribute to this elevated ellipticity through partial hybridization with the probe or with each other. However, increased ellipticity could also result from spectral overlap of the ssDNA signal at 280 nm, which would increase if scrambled sequences were retained through encapsulation in the hydrogel. Mixtures with the target sequence and multiple scrambled sequences displayed similar peak heights to those in alginate-dsDNA. Importantly, there was a greater distinction between the mixtures containing the target and those without for hydrogels containing the 2′-F modification. Notably, spectra of mixtures without the target sequence displayed peak heights similar to the ss 2′-F Oligo, while mixtures with the target sequence exhibited a blue-shifted peak (shift to 270 nm) with similar maxima to the probe + target duplex.

The addition of a mismatched sequence to larger mixtures was also investigated (Fig. S14) and produced spectra that mimicked the alginate-dsDNA spectrum, though with slightly elevated peak heights for both unmodified DNA and 2′-F Oligo (F-All$_{DNA}$). While slight differences were observed in the CD spectra, the variability introduced by the mixtures complicates definitive conclusions regarding the specificity of the hydrogel for the target sequence. However, PCA effectively separated hydrogels according to the presence of the target strand (Fig. 6). Dimension 1 clearly delineated spectra containing the target sequence from those without it, with greater separation observed for fluorine-modified samples. This is likely due to the increased differences in peak heights and greater shifts in CD peak maxima in samples containing the target sequence *versus* those without it. In fact, variation in dimension 1 was mainly attributed to wavelengths 242–247 nm and 269–276 nm (positive and negative CD maxima), further supporting these claims. Variation in dimension 2 was primarily attributed to wavelengths ranging from 251–265 nm (positive CD maxima for samples containing the target sequence).

3.4.1. Temperature melt (T_m) analysis. All mixtures containing target sequences displayed higher T_m values than their corresponding mixtures without the target (Table 3). The average difference in T_m values for mixtures with and without the target strand was 19 °C, which increased to 28 °C for fluorine-modified DNA. This suggests that the 2′-F Oligo (F-All$_{DNA}$) has stronger binding to the DNA target sequence, resulting in greater T_m differences and improved specificity. 2′-F nucleobase modifications are known to increase duplex stability by enhancing base stacking[28] and strengthening Watson–Crick base pairing.[22] In addition, 2′-F oligos offer significantly greater environmental stability compared to DNA-based sensors.[55] While DNA degrades over time,[56] studies indicate that 2′-F oligos are resistant to nucleases with enhanced stability,[55,57] making them promising candidates for long-lasting biosensors (Table 5).

3.4.2. Random forest classification. Random forest models were built using both CD spectra and temperature melt data, then used to classify samples according to the presence of the target sequence. We achieved high prediction accuracies when

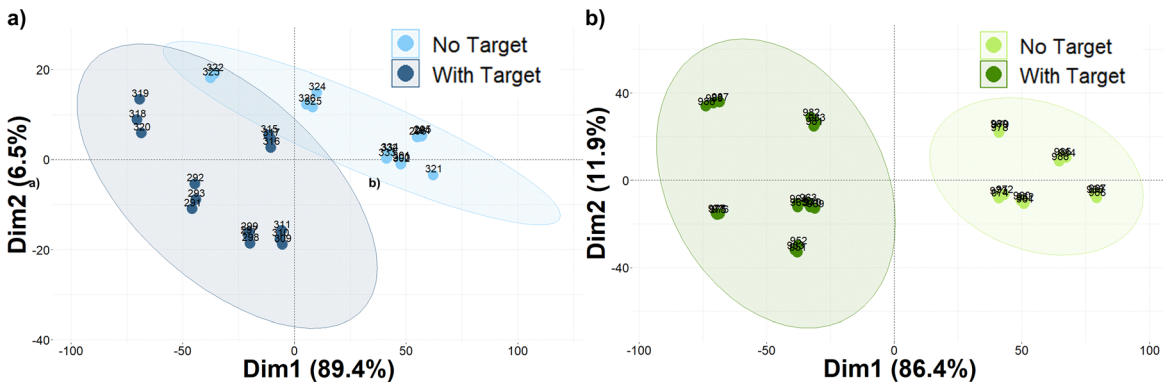

Fig. 6 PCA score plot from (a) DNA and (b) 2′-F Oligo (F-All$_{DNA}$) specificity study samples, excluding samples with mismatch sequence. Samples with the mismatch sequence were excluded, as it was previously established that the mismatch could partially bind to the Probe strand and form a duplex. PCA data were truncated to focus only on wavelengths in the oligonucleotide region of the spectra (230–290 nm) and were not normalized, as relative peak heights of mixtures compared to standard duplexes are important markers for discrimination between sample types.

Table 5 Averaged temperature melt values for DNA and 2′-F oligo samples

Sample contains	DNA T_m (°C)	2′-F Oligo T_m (°C)
DNA target	70	81
Mismatch	51	53
Mismatch + DNA target	74	83
Scrambled A	47	45
Scrambled A + DNA target	69	78
Scrambled B	58	56
Scrambled B + DNA target	76	81
Scrambled C	NA	52
Scrambled C + DNA target	73	79
Scrambled B + scrambled C	52	52
Scrambled B + scrambled C + DNA target	73	82
Scrambled A + scrambled B + scrambled C	56	NA
Scrambled A + scrambled B + scrambled C + DNA target	73	84
Mismatch + scrambled A	54	55
Mismatch + scrambled A + DNA target	72	83
Mismatch + scrambled A + scrambled B + scrambled C	57	58
Mismatch + scrambled A + scrambled B + scrambled C + DNA target	74	83

predicting classes of unknown (*i.e.*, withheld) data from the specificity studies. When only using CD data, we achieved a classification accuracy of 77% for unmodified DNA. When only using the temperature melt data, the accuracy decreased to 60%. However, when both datasets were combined using the average of the replicates, classification accuracy reached 83%. For the 2′-F Oligo (F-All$_{DNA}$), the accuracy was 90% when using only CD data and 48% when using only temperature melt data. When both datasets were combined, samples were correctly classified more than 95% of the time. These findings demonstrate that integrating CD spectra with temperature melt data enhances classification accuracy, particularly when dealing with complex mixtures containing similar sequences to those of the intended target. This is important, as we clearly demonstrate that 2′-fluoro nucleobase modifications significantly increase both sensitivity and target specificity without the need for amplification or complex and expensive labelling techniques.

4. Conclusion

We synthesized a label-free, amplification-free, and immobilization-free short oligonucleotide-based biosensor in which complement hybridization was detected and recorded using CD spectroscopy. We increased the sensitivity and specificity of our biosensor by adding a fluorine atom at the 2′ position of the oligonucleotide sugar. The changes in chirality due to conformational rearrangements could be observed in the CD spectra as an increase in peak height and shifts in peak maxima. The alginate-oligo hydrogels were synthesized using EDC/NHS coupling and CuAAC reactions. We first confirmed the synthesis of the alginate-azide hydrogel using FTIR, where we observed peaks attributed to the formation of an amide bond. Oligonucleotides were bound to the alginate-azide *via* CuAAC, and the products were isolated by centrifugal filtering. CD spectra were acquired to confirm the presence of DNA or RNA, and hybridization with the complement was observed through increased ellipticity and blue-shifted long-wavelength crossovers. Biosensors displayed great sensitivity with limits of detection of 2.9 nmol and 2.1 nmol for 2′F DNA- and RNA-based sensors, respectively, surpassing their unmodified counterparts in the case of DNA. The 2′F modified oligo biosensor was also shown to be more specific for its target complementary sequence than the unmodified version when placed in mixtures with several non-complementary strands. Chemometric models combining CD spectra with temperature melt data demonstrated higher classification accuracies for fluorine-modified DNA (95%) than its unmodified counterpart (83%). Although CD spectroscopy is not traditionally known to be a technique that can discriminate between samples with similar composition, we have demonstrated that it is possible to do so by pairing it with chemometrics. We have demonstrated that it is possible to synthesize highly sensitive and specific biosensors by modifying nucleobases within the DNA/RNA probe strand, and detecting hybridization without the need for traditional complex approaches like amplification, labelling, or immobilization. Future work should focus on improving discrimination between the target strand and strands containing similar sequences with a few mismatches in more complex sample matrices.

Author contributions

The manuscript was written through contributions of all authors. All authors have given approval to the final version of the manuscript.

Conflicts of interest

The authors declare no competing financial interest.

Abbreviations

°C	Degrees Celsius
CD	Circular dichroism
CuAAC	Copper-(I) catalyzed azide–alkyne cycloaddition
ds	Double stranded

EDC	1-Ethyl-3-(-3-dimethylaminopropyl) carbodiimide hydrochloride
FTIR	Fourier Transform Infrared
G'	Storage modulus
G''	Loss modulus
LVE	Linear viscoelastic range
NHS	N-Hydroxysuccinimide
NIST	National Institute of Standards and Technology
nm	Nanometers
nM	Nanomole
NMR	Nuclear magnetic resonance
OD	Optical density
SRM	Standard reference materials
ss	Single stranded
UV-Vis	Ultraviolet-visible

Data availability

The data supporting this article have been included as part of the supplementary information (SI). Supplementary information: additional spectroscopic and rheological characterization, a full list of sample names and additional PCAs. See DOI: https://doi.org/10.1039/d5tb02880a.

Acknowledgements

We are thankful for the funding support to conduct this research. This work was supported by the Natural Sciences and Engineering Research Council of Canada (NSERC) Discovery and Discovery Accelerator Supplement Grants (RGPIN-2020-05816) awarded to TS and NSERC Discovery (RGPIN-2019-04692) awarded to JPD. Author DL received the Ontario Tech University Student Training Assistantships in Research (STAR) and is currently supported through the Graduate International Tuition Scholarship (GITS). Author CE is currently supported through the NSERC CGS-D program. Thank you to Dr. Matthew Hammill for his help with the synthesis of the DNA and RNA sequences.

References

1 A. P. Turner, Biosensors: sense and sensibility, *Chem. Soc. Rev.*, 2013, **42**(8), 3184–3196.
2 Y. Hua, J. Ma, D. Li and R. Wang, DNA-based biosensors for the biochemical analysis: a review, *Biosensors*, 2022, **12**(3), 183.
3 P. Bhalla and N. Singh, Generalized Drude scattering rate from the memory function formalism: an independent verification of the Sharapov–Carbotte result, *Eur. Phys. J. B*, 2016, **89**, 1–8.
4 J.-K. Chen, G.-Y. Zhou, C.-J. Chang and C.-C. Cheng, Label-free detection of DNA hybridization using nanopillar arrays based optical biosensor, *Sens. Actuators, B*, 2014, **194**, 10–18.
5 J. Bush, C.-H. Hu and R. Veneziano, Mechanical properties of DNA hydrogels: towards highly programmable biomaterials, *Appl. Sci.*, 2021, **11**(4), 1885.
6 X. Hu, L. Zhang, L. Yan and L. Tang, Recent advances in polysaccharide-based physical hydrogels and their potential applications for biomedical and wastewater treatment, *Macromol. Biosci.*, 2022, **22**(9), 2200153.
7 A. Orr, P. Wilson and T. Stotesbury, DNA-crosslinked alginate hydrogels: characterization, microparticle development, and applications in forensic science, *ACS Appl. Polym. Mater.*, 2022, **5**(1), 583–592.
8 Y. Wang, Y. Zhang, Q. Zhang, X. Li, Q. Yan and Y. Zhu, Mechanical properties modulation and biological applications of DNA hydrogels, *Adv. Sens. Energy Mater.*, 2024, **3**(3), 100113.
9 J. Gačanin, C. V. Synatschke and T. Weil, Biomedical applications of DNA-based hydrogels, *Adv. Funct. Mater.*, 2020, **30**(4), 1906253.
10 I. Y. Jung, E. H. Lee, A. Y. Suh, S. J. Lee and H. Lee, Oligonucleotide-based biosensors for in vitro diagnostics and environmental hazard detection, *Anal. Bioanal. Chem.*, 2016, **408**(10), 2383–2406, DOI: 10.1007/s00216-015-9212-2.
11 A. Toldrà, C. Alcaraz, J. Diogène, C. K. O'Sullivan and M. Campàs, Detection of ostreopsis cf. ovata in environmental samples using an electrochemical DNA-based biosensor, *Sci. Total Environ.*, 2019, **689**, 655–661.
12 I. Y. Jung, J. B. You, B. R. Choi, J. S. Kim, H. K. Lee, B. Jang, H. S. Jeong, K. Lee, S. G. Im and H. Lee, A highly sensitive molecular detection platform for robust and facile diagnosis of middle east respiratory syndrome (MERS) corona virus, *Adv. Healthcare Mater.*, 2016, **5**(17), 2168–2173, DOI: 10.1002/adhm.201600334.
13 P. Moitra, M. Alafeef, K. Dighe, M. B. Frieman and D. Pan, Selective naked-eye detection of SARS-CoV-2 mediated by N gene targeted antisense oligonucleotide capped plasmonic nanoparticles, *ACS Nano*, 2020, **14**(6), 7617–7627.
14 L. K. McGoldrick and J. Halámek, Recent advances in noninvasive biosensors for forensics, biometrics, and cybersecurity, *Sensors*, 2020, **20**(21), 5974.
15 X. Hai, Y. Li, C. Zhu, W. Song, J. Cao and S. Bi, DNA-based label-free electrochemical biosensors: from principles to applications, *TrAC, Trends Anal. Chem.*, 2020, **133**, 116098.
16 T. Endo, K. Kerman, N. Nagatani, Y. Takamura and E. Tamiya, Label-free detection of peptide nucleic acid–DNA hybridization using localized surface plasmon resonance based optical biosensor, *Anal. Chem.*, 2005, **77**(21), 6976–6984.
17 Z. Chen, K. Mao, J. Xue, R. Feng, K. Zhang, J. Su, W. Du, J. Ran, C. Yang and Z. Yang, *et al.*, Development and application of DNA hydrogels in biosensing: Current status and future implications, *Microchem. J.*, 2025, **213**, 113664, DOI: 10.1016/j.microc.2025.113664.
18 Y. Chen, C. Qian, C. Liu, H. Shen, Z. Wang, J. Ping, J. Wu and H. Chen, Nucleic acid amplification free biosensors for pathogen detection, *Biosens. Bioelectron.*, 2020, **153**, 112049.
19 M. Sidstedt, P. Rådström and J. Hedman, PCR inhibition in qPCR, dPCR and MPS—mechanisms and solutions, *Anal. Bioanal. Chem.*, 2020, **412**(9), 2009–2023.

20 G. Fazakerley, S. Uesugi, A. Izumi, M. Ikehara and W. Guschlbauer, A→ Z transition in the synthetic hexanucleotide (dCdGfl) 3, *FEBS Lett.*, 1985, **182**(2), 365–369.
21 H. Ikeda, R. Fernandez, J. J. Barchi Jr, X. Huang, V. E. Marquez and A. Wilk, The effect of two antipodal fluorine-induced sugar puckers on the conformation and stability of the Dickerson-Drew dodecamer duplex [d (CGCGAATTCGCG)] 2, *Nucleic Acids Res.*, 1998, **26**(9), 2237–2244.
22 M. Manoharan, A. Akinc, R. K. Pandey, J. Qin, P. Hadwiger, M. John, K. Mills, K. Charisse, M. A. Maier and L. Nechev, Unique gene-silencing and structural properties of 2′-fluoro-modified siRNAs, *Angew. Chem.*, 2011, **123**(10), 2332–2336.
23 T. P. Prakash, An overview of sugar-modified oligonucleotides for antisense therapeutics, *Chem. Biodiversity*, 2011, **8**(9), 1616–1641.
24 A. Khvorova and J. K. Watts, The chemical evolution of oligonucleotide therapies of clinical utility, *Nat. Biotechnol.*, 2017, **35**(3), 238–248.
25 U. Heinemann and Y. Roske, Symmetry in nucleic-acid double helices, *Symmetry*, 2020, **12**(5), 737.
26 M. Evich, A. M. Spring-Connell and M. W. Germann, Impact of modified ribose sugars on nucleic acid conformation and function, *Heterocycl. Commun.*, 2017, **23**(3), 155–165.
27 J. K. Watts, N. Choubdar, K. Sadalapure, F. Robert, A. S. Wahba, J. Pelletier, B. M. Pinto and M. J. Damha, 2′-fluoro-4′-thioarabino-modified oligonucleotides: conformational switches linked to siRNA activity, *Nucleic Acids Res.*, 2007, **35**(5), 1441–1451, DOI: 10.1093/nar/gkl1153.
28 F. Guo, Q. Li and C. Zhou, Synthesis and biological applications of fluoro-modified nucleic acids, *Org. Biomol. Chem.*, 2017, **15**(45), 9552–9565, DOI: 10.1039/c7ob02094e.
29 A. Patra, M. Paolillo, K. Charisse, M. Manoharan, E. Rozners and M. Egli, 2′-Fluoro RNA shows increased Watson–Crick H-bonding strength and stacking relative to RNA: evidence from NMR and thermodynamic data, *Angew. Chem., Int. Ed. Engl.*, 2012, **51**(47), 11863–11866, DOI: 10.1002/anie.201204946.
30 E. A. Lesnik, C. J. Guinosso, A. M. Kawasaki, H. Sasmor, M. Zounes, L. L. Cummins, D. J. Ecker, P. D. Cook and S. M. Freier, Oligodeoxynucleotides containing 2′-O-modified adenosine: synthesis and effects on stability of DNA: RNA duplexes, *Biochemistry*, 1993, **32**(30), 7832–7838.
31 K. Y. Lee and D. J. Mooney, Alginate: properties and biomedical applications, *Prog. Polym. Sci.*, 2012, **37**(1), 106–126, DOI: 10.1016/j.progpolymsci.2011.06.003.
32 S. Liparoti, V. Speranza and F. Marra, Alginate hydrogel: the influence of the hardening on the rheological behaviour, *J. Mech. Behav. Biomed. Mater.*, 2021, **116**, 104341.
33 X. Guo, Y. Wang, Y. Qin, P. Shen and Q. Peng, Structures, properties and application of alginic acid: A review, *Int. J. Biol. Macromol.*, 2020, **162**, 618–628.
34 H. J. Kong, D. Kaigler, K. Kim and D. J. Mooney, Controlling rigidity and degradation of alginate hydrogels via molecular weight distribution, *Biomacromolecules*, 2004, **5**(5), 1720–1727.
35 C. Zhang, R. Grossier, N. Candoni and S. Veesler, Preparation of alginate hydrogel microparticles by gelation introducing cross-linkers using droplet-based microfluidics: a review of methods, *Biomater. Res.*, 2021, **25**(1), 41.
36 M. A. LeRoux, F. Guilak and L. A. Setton, Compressive and shear properties of alginate gel: effects of sodium ions and alginate concentration, *J. Biomed. Mater. Res.*, 1999, **47**(1), 46–53.
37 E. M. Ahmed, Hydrogel: Preparation, characterization, and applications: a review, *J. Adv. Res.*, 2015, **6**(2), 105–121.
38 H. Jaganathan, J. M. Kinsella and A. Ivanisevic, Circular dichroism study of the mechanism of formation of DNA templated nanowires, *ChemPhysChem*, 2008, **9**(15), 2203–2206, DOI: 10.1002/cphc.200800509.
39 P. Shi, N. Zhao, J. Coyne and Y. Wang, DNA-templated synthesis of biomimetic cell wall for nanoencapsulation and protection of mammalian cells, *Nat. Commun.*, 2019, **10**(1), 2223, DOI: 10.1038/s41467-019-10231-y.
40 S. I. Presolski, V. P. Hong and M. G. Finn, Copper-catalyzed azide-alkyne click chemistry for bioconjugation, *Curr. Protoc. Chem. Biol.*, 2011, **3**(4), 153–162, DOI: 10.1002/9780470559277.ch110148.
41 N. Rahman and S. Khan, Circular dichroism spectroscopy: a facile approach for quantitative analysis of captopril and study of its degradation, *ACS Omega*, 2019, **4**(2), 4252–4258.
42 M. Santos-Cancel and R. J. White, Collagen membranes with ribonuclease inhibitors for long-term stability of electrochemical aptamer-based sensors employing RNA, *Anal. Chem.*, 2017, **89**(10), 5598–5604, DOI: 10.1021/acs.analchem.7b00766.
43 D. M. Gray; R. L. Ratliff and M. R. Vaughan, [19] Circular dichroism spectroscopy of DNA, in *Methods in Enzymology, Vol. 211*, Academic Press, 1992, pp. 389–406.
44 P. Paul and G. Suresh Kumar, Thionine interaction to DNA: comparative spectroscopic studies on double stranded *versus* single stranded DNA, *J. Fluoresc.*, 2012, **22**(1), 71–80, DOI: 10.1007/s10895-011-0931-2.
45 M. Hammill, The synthesis and *in vitro* evaluation of chemically modified siRNAs that contain internal azobenzene derivative spacers for selective and tunable photocontrol of activity, PhD thesis, Ontario Tech University, 2017.
46 J. Kypr, I. Kejnovská, D. Renčiuk and M. Vorlíčková, Circular dichroism and conformational polymorphism of DNA, *Nucleic Acids Res.*, 2009, **37**(6), 1713–1725.
47 M. B. Arghavani, J. SantaLucia and L. J. Romano, Effect of mismatched complementary strands and 5′-change in sequence context on the thermodynamics and structure of benzo[*a*]pyrene-modified oligonucleotides, *Biochemistry*, 1998, **37**(23), 8575–8583.
48 N. Kakiuchi, C. Marck, N. Rousseau, M. Leng, E. De Clerq and W. Guschlbauer, Polynucleotide helix geometry and stability. Spectroscopic, antigenic and interferon-inducing properties of deoxyribose-, ribose-, or 2′-deoxy-2′-fluoro-ribose-containing duplexes of poly(inosinic acid). poly(cytidylic acid), *J. Biol. Chem.*, 1982, **257**(4), 1924–1928, DOI: 10.1016/S0021-9258(19)68127-5.
49 M. N. Islam, M. K. Masud, M. H. Haque, M. S. A. Hossain, Y. Yamauchi, N. T. Nguyen and M. J. Shiddiky, RNA biomarkers: diagnostic and prognostic potentials and recent

developments of electrochemical biosensors, *Small Methods*, 2017, **1**(7), 1700131.

50 J. Wang and N. Hui, Electrochemical functionalization of polypyrrole nanowires for the development of ultrasensitive biosensors for detecting microRNA, *Sens. Actuators, B*, 2019, **281**, 478–485.

51 M. Bolourinezhad, M. Rezayi, Z. Meshkat, S. Soleimanpour, M. Mojarrad, S. H. Aghaee-Bakhtiari and S. M. Taghdisi, Design of a rapid electrochemical biosensor based on MXene/Pt/C nanocomposite and DNA/RNA hybridization for the detection of COVID-19, *Talanta*, 2023, **265**, 124804.

52 C. Fan, K. W. Plaxco and A. J. Heeger, Electrochemical interrogation of conformational changes as a reagentless method for the sequence-specific detection of DNA, *Proc. Natl. Acad. Sci. U. S. A.*, 2003, **100**(16), 9134–9137.

53 X. Lu, X. Dong, K. Zhang, X. Han, X. Fang and Y. Zhang, A gold nanorods-based fluorescent biosensor for the detection of hepatitis B virus DNA based on fluorescence resonance energy transfer, *Analyst*, 2013, **138**(2), 642–665, DOI: 10.1039/c2an36099c.

54 R. Hu, T. Liu, X.-B. Zhang, S.-Y. Huan, C. Wu, T. Fu and W. Tan, Multicolor fluorescent biosensor for multiplexed detection of DNA, *Anal. Chem.*, 2014, **86**(10), 5009–5016, DOI: 10.1021/ac500618v.

55 M. Sanroman-Iglesias, C. H. Lawrie, L. M. Liz-Marzan and M. Grzelczak, The role of chemically modified DNA in discrimination of single-point mutation through plasmon-based colorimetric assays, *ACS Appl. Nano Mater.*, 2018, **1**(7), 3741–3746.

56 C. Xue, H. Huang, L. Wang, W. Liao, H. Jiang and Z.-S. Wu, Swelling of serum-stable DNA nanoparticles upon target-induced conformational rearrangement of sensing probes for the signal-on detection of cancer-related genes, *Anal. Chem.*, 2022, **94**(6), 2749–2756.

57 J. Lietard, H. Abou Assi, I. Gomez-Pinto, C. González, M. M. Somoza and M. J. Damha, Mapping the affinity landscape of Thrombin-binding aptamers on 2′ F-ANA/DNA chimeric G-Quadruplex microarrays, *Nucleic Acids Res.*, 2017, **45**(4), 1619–1632.